

# A study of pulsed thermography for life assessment of thin EB-PVD TBCs undergoing oxidation ageing

Lawrence Tinsley<sup>a,\*</sup>, Christine Chalk<sup>a</sup>, John Nicholls<sup>a</sup>, Jörn Mehnen<sup>b</sup>, Rajkumar Roy<sup>a</sup>

<sup>a</sup> Through-life Engineering Services Centre, Cranfield University, MK43 0AL, UK

<sup>b</sup> Dept. of Design, Manufacture and Engineering Management, University of Strathclyde, 75 Montrose St, Glasgow, Scotland, G1 1XJ, UK

## ARTICLE INFO

### Keywords:

Pulse thermography  
Thermal Barrier Coating  
Thermal diffusivity  
Oxidation ageing

## ABSTRACT

This paper presents an assessment of ageing for thin Thermal Barrier Coatings (TBC) using active thermography. As TBCs undergo ageing during their service life, sintering changes the porosity, elements migrate from the substrate, and micro-cracks build up in the structure of the material, exhibiting a change in thermal conductivity and diffusion properties. As the material ages and these properties change over time, it is possible to exploit trends in this change for characterisation of coating ageing, which would provide a diagnostics tool to estimate remaining useful life. In this study, through-depth diffusivity measurement has been applied to thin EB-PVD coatings which are artificially aged via oxidation furnace cycles. In order to address the difficulties of capturing a fast thermal event in a thin coating, a novel parametric study approach has been carried out to optimise data capture and analysis, maximising available frames for the model fitting step. Through-depth diffusivities have been measured during ageing for six samples, yielding a repeatable trend in thermal diffusivity measurements, with three features, which can be exploited for ageing characterisation of thin EB-PVD TBCs, and used as an alarm of imminent failure.

## 1. Introduction

The performance and durability of gas turbines have been significantly increased with the application of Thermal Barrier Coatings (TBCs), which help protect components from the intense heat from combustion gases. The coatings reduce the temperature of the surface of the allowing higher temperature operation with improved efficiency.

Over the last decade there has been considerable research in the application of thermography to the non-destructive testing (NDT) of TBC. This has primarily seen application in the detection of delaminations, monitoring of residual stresses at the interface boundary, and more recently in the assessment of ageing through measurement of thermo-physical property with a particular focus on thick air plasma spray (APS) coatings. The aim of this study is to demonstrate the applicability of the thermographic technique to thin Electron Beam Physical Vapour Deposition (EB-PVD) coatings, and explore the difficulties with its practical application. In order to address these difficulties, various data capture parameters need to be explored in a parametric study, as well as analysis parameters to maximise frame inclusion without flash afterglow or back wall effects.

It is the aim of this experiment to explore and overcome difficulties

with a fast thermal event, and to identify and test exploitable trends in the relationship between the thermophysical property of thin EB-PVD TBCs and age, as measured by single-sided thermography, to qualify a test for measuring remaining life of TBCs.

## 2. Background

### 2.1. Thermal Barrier Coatings, sintering and spallation

TBCs are coatings of insulating materials used in aero engine and gas turbines, made from a ceramic, which function to reduce the temperature from the surrounding gases that the coated component is subjected to by up to 50–150 °C [1]. These are typically applied by air plasma spray (APS) or electron beam physical vapour deposition (EB-PVD), the structure of which is shown in Fig. 1. During the component service life, the components are placed under a variety of conditions which cause ageing to the materials. These factors include high stresses both thermal and mechanical; vibration, and contamination. The usual failure mechanism of TBCs is related to oxidation-driven spallation at the interface either between the oxide scale layer, known as Thermally Grown Oxide (TGO), and the bond coat, or between the TGO and the ceramic topcoat,

\* Corresponding author.

E-mail address: [l.tinsley@cranfield.ac.uk](mailto:l.tinsley@cranfield.ac.uk) (L. Tinsley).

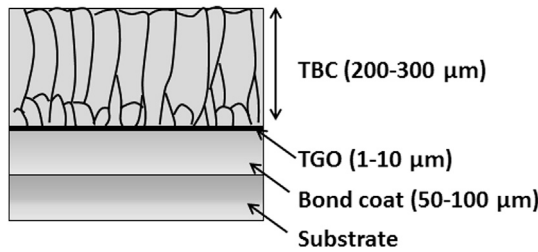


Fig. 1. Structure of a typical EB-PVD TBC.

where crack and spallation in the oxide layer between the bond coat and ceramic top coat can grow until failure of the coating. A mechanistic approach has been developed to improve the prediction of TBC life in this regard, with particular focus on the physics of stresses driving the nucleation of cracking at the TGO level, which requires knowledge of the TBC's morphology and service conditions endured [2].

A life prediction method has been developed by Beck et al. [3] based on TGO crack growth kinetics, taking into account minimum and maximum temperatures of thermal cycling, as well as dwell time at maximum temperature, however this approach provides a prognostic method, and is not useful for in-service diagnostics.

Other research by Pint et al. [4] takes a different approach and studies migration of elements between the substrate and the TGO, and the resulting stresses in the layer, where Aluminium can diffuse and lead to the formation of other oxides, and Nickel may be more susceptible to the formation of voids, leading to spallation at the interface. Other elements in the alloy can migrate more easily. Between these different mechanisms, a bond coat may function in allowing oxide scale formation, but may also be more prone to formation of voids. There are multiple drivers behind TBC failure relating to the structure of coating, the material used, its thermal cycling, minimum and maximum temperature, and mechanical loading. These developments are useful in providing an estimate of TBC life on various designs and the dominant factors in well-known service conditions, however, it would be challenging to apply their approach in a service context.

Meanwhile, the life prediction methodology by Busso et al. [2] provides a method to facilitate in-situ life inspections. However, it also has challenges in requiring various inputs to be known, including full description of the TBC and its interface roughness, including the thermal cycling that the part has been subjected to.

## 2.2. Diffusivity-based ageing characterisation

A variety of research has been conducted on the topic of categorising the remaining useful life of TBCs. There is a requirement in industry to evaluate TBC ageing in-situ during their service life to predict remaining useful life and improve decisions at maintenance intervals. Measurement of stresses or change in material properties can facilitate this need.

Bison, Cernuschi, Grinzato, Marinetti & Robba [5] developed a thermographic inspection technique to estimate in-plane and in-depth thermal diffusivity measurements of TBCs, which was applied for through-thickness measurement of APS TBCs, anticipating no difference between the directions. This was later applied to measurement of both in-plane and through-thickness of APS TBCs [6], and then to APS TBCs that were subjected to furnace oxidation cycling [7,8]. As these studies were targeting a niche area of NDT not covered by other techniques, such as Photo Luminescence Piezo Spectroscopy [9], they focused on APS TBCs between 300 and 400 μm in thickness, leaving thin EB-PVD TBCs less than 200 μm thick to other techniques.

## 3. Experimental setup

Thermophysical material properties are typically measured using the Flash Method [10]. In this experiment, the front-face flash method is

applied, with a 1-dimensional thermal model fitted to the data, allowing estimation of the surface coating diffusivity.

The samples were exposed to furnace oxidation on a basis of time at temperature. These were artificially aged over time at over 1100 °C for up to 128 h in 16 h intervals, as this provides 8 stages for testing during the coating life in addition to the initial state. Pulsed thermographic data was taken at each interval of the experiment in order to capture changes in thermal diffusivity of the TBC. The thermographic system used for heat application and camera-flash synchronisation was Thermoscope®II by Thermal Wave Imaging Inc. [11]. The infrared radiometer used alongside this system for the data capture was a FLIR SC7600 series model. The radiometer hosts an Indium Antimonide sensor which possesses a full spatial resolution of 640 × 512 pixels, in the spectral range of 3–5.1 mm in the Mid Wave Infrared spectrum, and noise equivalent temperature difference of 20 mK. The data capture setup involved the placing of the sample on a fixture which was located in front of an internally reflective flash hood containing two Xenon flash bulbs which deliver a short light burst of approximately 2 kJ and 4 ms in length, with the radiometer facing the sample through an open observation window at a distance of 230 mm from the sample. This setup is shown in Fig. 2.

One of the advantages relating to data capture with the Thermoscope system, is that it synchronises frame captures with the triggering of the flash system, which helps overcome long-standing issues in pulse thermography about uncertainty of the timing of the flash pulse in relation to the surrounding frames. However, in order to accurately obtain a measure of diffusivity from the data, it is important to cut the correct segment of the data sequence for the model to fit. Firstly, an offset is required to initiate the data sequence after the flash and its immediate afterglow, and second is the requirement for a frame “window” limit, so that the later frames in the sequence fed to the model fitting do not contain a second inflection point where the heat pulse reaches the back wall of the substrate. This window is shown in Fig. 3.

### 3.1. Two-layer thermal model

A one-dimensional model for the cooling of a uniformly heated, semi-infinite 2-layer system is fitted to the measured temperature evolution over time (1). This is fitted by a non-linear best fit, returning an estimation of diffusivity, effusivity, thickness and coefficient of reflection, depending on what is known and what is desired [12].

$$T(t) = \frac{Q_0}{\varepsilon_c \sqrt{\pi t}} \left[ 1 + 2 \sum_{n=1}^{\infty} \Gamma^n e^{-\frac{n^2 l_c^2}{\alpha_c t}} \right] \quad (1)$$

where  $\varepsilon = \sqrt{k\rho Cp}$  is the effusivity in W/cm<sup>2</sup>/K/s<sup>0.5</sup>,  $\Gamma = (\varepsilon_c - \varepsilon_s)/(\varepsilon_c + \varepsilon_s)$  is the reflection coefficient between the coating (c) and substrate (s), and  $l_c$  refers to coating thickness.  $\alpha_c$  is coating diffusivity in m<sup>2</sup>/s,  $t$  is the time after the flash pulse, in seconds.

### 3.2. Samples

Experiments were performed on six samples of identical design. The

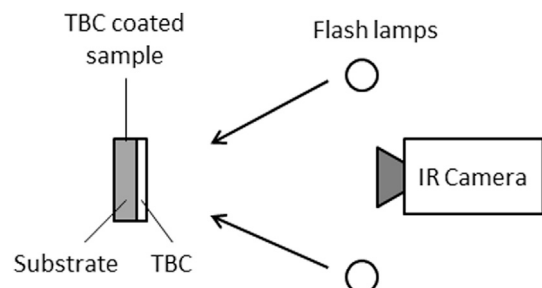


Fig. 2. Thermographic data capture experimental setup.

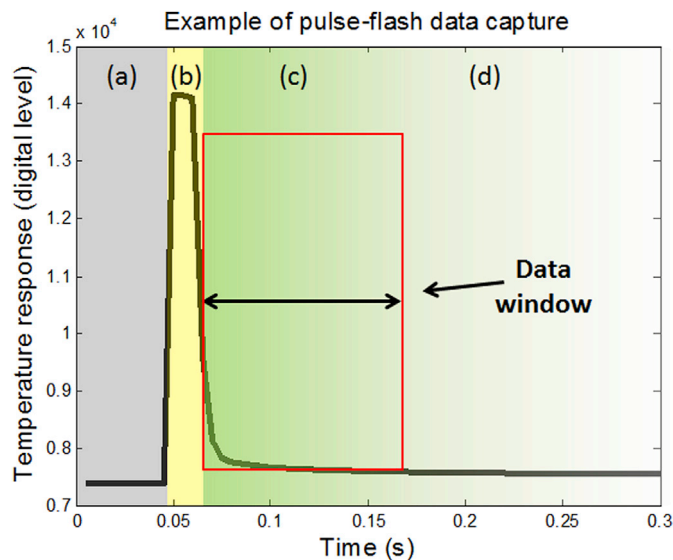


Fig. 3. Illustration of the data output showing different regions within the data, from pre-flash (a), flash duration and post-flash heating effects (b), coating data window (c) and heat pulse diffusion into the substrate material (d).

samples were made with a platinum diffused bond coat, the ceramic was Zirconia-7wt. % Yttria topcoat deposited via Electron Beam Physical Vapour Deposition, of uniform thickness of approximately 150  $\mu\text{m}$ . The substrate used was CMSX-4.

### 3.3. Parametric study

A key issue of the experiment involves the wide range of parameters that affect the temperature readings feeding into the diffusivity estimation. The full number of factors could be extensive, depending on the available equipment. A laser heat source can have a more carefully controlled heat duration than flash lamps, and a shorter pulse, which in the ideal case modelled in equation (1) would require a higher energy or a more intense beam to facilitate high energy input in a shorter burst. In literature, the setup description of an experiment is usually sufficient to allow an approximate replication; however, some factors, such as integration time of the detector, and the parameters of the exact data window within the full data capture, are not usually disclosed, resulting in some ambiguity which would usually be filled with direct information requests or educated guesses on which parameters would be ideal. Even then, a narrow selection of parameters without comparison is likely, and there is an uncertainty on the settings of the inputs, and how the resulting output may compare with parallel experiments with parametric variation.

From the equipment available, the experiment entailed 5 key factors, each with varying number of levels available for selection with each, which are: (a) integration time of the infrared detector, which is the equivalent of exposure time for a photographic camera, in this case referring to the exposure time before read-out of a shutter free detector, (b) the flash power intensity, which in this case is a % of maximum power intensity, referring to the % of the capacitor bank's full output used for the flash pulse, (c) the application of a soot coating to the surface to improve emissivity, which is usually applied in all experiments considering the translucency of TBCs in infrared and visible light [13,14], however it is desirable for real-world tests to forego this requirement, and (d) the beginning and (e) end of the data window that is used for the calculation. The last two factors are important at the analysis stage because of difficulty in determining the termination of the flash and its afterglow, as well as the need with a fast thermal event to use a sufficient number of frames for calculation.

#### 3.3.1. Data window

For flash lamp heat sources, the termination of the heat pulse and

beginning of the coating's thermal diffusion is uncertain. The window limit introduces an uncertainty where it is logically sound to select an arbitrary point beyond the heat pulse encountering and crossing into the substrate. However, owing to the model-fitting methodology, or the polynomial fitting of the TSR peak second differential method [15], it is important to have abundant data covering both sides of the transition while not using frames affected by the termination of the substrate. Usually for thick coatings and large substrates with slow thermal events, making an educated selection based on calculations is sufficient. However, with thin coating inspection, while the substrate is much thicker in comparison, in terms of diffusion time through a highly conductive metal, both layers experience a fast thermal event for obtainable framerates. Seeking the optimum data window for calculating the diffusivity is a key exercise. With only a few dozen frames within the diffusion time available at accessible framerates, any initial frame still in the flash pulse will result in under fitting the solution to the data. A low number of frames beyond the coating-substrate interface will increase the effect of noise and result in a poor fit, while excess frames beyond the interface would encounter the influence of the rear surface of the substrate. In order to identify the correct data window, as well as setup parameters, a design of experiments methodology was adopted.

#### 3.3.2. Design of experiments

The 5 key factors were used as inputs. The trend sought was a stable point in the output of thermal diffusivity estimation and a high coefficient of determination,  $R^2$ . From the equipment used, a full-factorial experiment with all possible levels included would be very large. Thousands of levels of integration times are available in custom specification, while there are several flash power options available in the Thermoscope II™ system. Initially limiting (a) integration time to 5 levels – the calibrated default, surrounded by four 1000  $\mu\text{s}$  steps spread either side – (b) the flash power to four wide steps, (c) application of soot coating on/off, (d) 5 frame offsets after the flash of 0–4 and (e) window size from 10 to 40 frames (31 levels), initially reduces the number of experiments to a partial factorial of 40 experiments per sample, and 6200 outputs, factoring all analysis parameters (d) and (e). This can be reduced further by limiting the number of window limit parameters to a handful of steps spread within 10–40 frames. The steps chosen were finer within the first 10 frames to capture initial variation of the output, which should begin reaching stability beyond 20 frames as both sides of the interface boundary come to be held in the data window, and as extra steps are added in steps of 10 frames (50 ms) beyond that, it is expected for the output to shift from that stable region. With 0 and 1 frame offset, starting the data window at the flash frame timestamped by the Mosaic system, and 5 ms after the flash: these are expected to vary their output measurements significantly, as the flash duration and afterglow will dominate the fitting of eq. (1). The partial factorial setup reflecting this parameter reduction is shown in Table 1. Integration time is the time duration that the pixels on the detector chip are exposed to incident radiation before refresh and data readout. An issue with performing high framerate inspection is that in order to obtain a high framerate, the maximum framerate is limited by the integration time used; the longer the integration time, the lower the maximum framerate available. In all experiments, the framerate of 200 Hz was used, as this was the maximum achievable framerate of the longest integration time, and would be available to all experiments, eliminating it as a factor. In order to achieve this framerate,  $\frac{1}{4}$  windowing mode was used. Longer integration times would reduce the maximum framerate, while lower framerates would reduce the amount of data available to fit the model to.

The resulting inputs and levels would produce 40 physical experiments, with 35 analysis variations on each, yielding 1400 outputs for a single set of tests for one sample at each point in the experiment. The partial factorial experiment design was run for a single sample before the furnace cycling stage to reduce the total number of experiments. In the initial stage, 54 experiments were conducted, which included variations of parameters and their levels in Table 1. In addition to the identified

**Table 1**

Design of experiments matrix for parametric study – gaps indicate no additional levels selected, as different factors have different levels available.

Index	Factor	Units	Level (1)	Level (2)	Level (3)	Level (4)	Level (5)	Level (6)	Level (7)
A	Integration time	μs	1000	2000	2271	3000	4000	–	–
B	Flash intensity	% max power	25	50	75	100	–	–	–
C	Soot coating	applied	No	Yes	–	–	–	–	–
D	Frame offset	number	0	1	2	3	4	–	–
E	Window limit	number	10	12	14	16	20	30	40

factors, a handful of ‘soft’ factors, such as the effects of different waiting time between captures, to offset heat build-up within the flash hood; and data captures at different times of day with changes in ambient temperature and humidity in the lab environment. The soft factors tested produced no measurable effects.

### 3.4. Furnace cycling TBCs

Having condensed the number of factors, the samples were inspected at each stage of the experiment from initial pre-exposure to every stage between the 16 h cycles, until the onset of coating spallation. At each stage, samples were removed from the furnace, left to cool for 15 min, at which point they had cooled to approx. 60 °C, and were quenched in distilled water. The samples were subjected to a thermographic inspection without then with a graphite soot coating applied to increase emissivity of the surface. This soot coating was partially removed with water in an ultrasonic bath then isopropanol in an ultrasonic bath, and returned to the furnace. Any soot residue would be vaporised in the furnace, leaving the samples clean and uncontaminated for the next soot-free inspection stage. The full cycle of this process is shown in Fig. 4.

## 4. Results

### 4.1. Parametric study

A single experiment of the parametric study is shown in Fig. 5, where

a single data capture is stretched over its 35 analysis iterations, with every set of several data points representing each of five offset values between 0 and 4; and within each offset subset are the window limits from Table 1. The full results of this parametric study are shown in Fig. 6, which displays the output estimation of thermal diffusivity against the partial factorial parameters, as well as other variations discussed above. The objective of this exercise being to seek out parameter combinations which achieve stable regions of diffusivity estimation without significant variation or noise. As the parameters approach optimal settings, the output stabilises, giving an optimal solution where the outputs show little variability with adjustment of factor levels, as seen in Fig. 5. In the figure, offset and window limit parameters are varied along the x-axis, where every several points along the axis are the window variations between 10 and 40, within each set for offset parameter, 0–4, from left to right.

This allows selection of optimum analysis parameter combinations that result in stable regions of results, seen here in the center set (circled), indicating first that offset is a very strongly influential factor, showing strong variations from left (offset of 0) to right (4); with window limit also having a strong influence, within each offset subset. As the estimations for offset of 2 indicate, the influence of window limit is significantly reduced with the optimum offset value, achieving a stable region where  $R^2$  coefficient is high, and diffusivity measurement has a low variation within the offset setting. This was consistently found not to be the case with all other offset values. This also held further to experiments with variations of the other factors, giving a full variation in the outputs, shown in Fig. 6. In the figure, many experiments were performed with

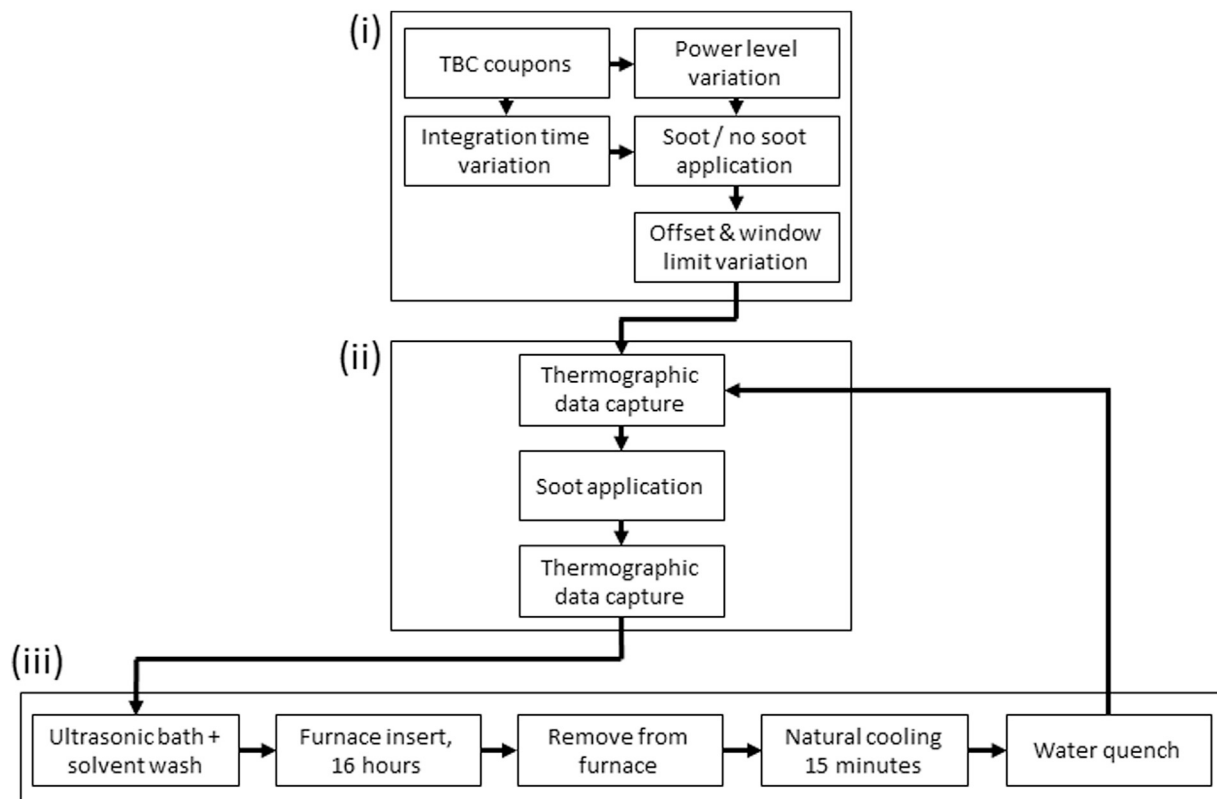


Fig. 4. Flowchart of inspection process during the furnace cycle. The process repeats until the TBC spalls in either of the last two steps of stage (iii).



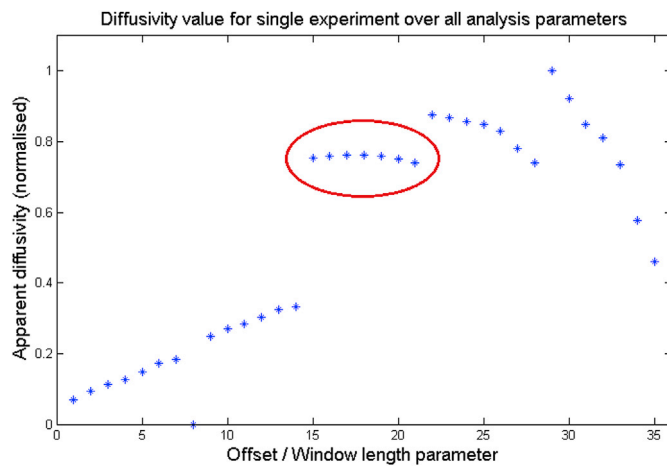


Fig. 5. Comparison of analysis parameters (x-axis) against their resulting diffusivity measurement in a single data capture at one integration time and flash power.

experimental parameter variations along the y-axis, while each set of several points along the x-axis represent each of the window variations for each level of offset value. The first seven points along the x-axis containing data for offset of 0, with frame limits of 10, 12, 14, 16, 20, 30, 40, allowing both classes of parameters to be compared.

In this way, the other factors can be interrogated for the variance of their outputs and can also be tested according to the coefficient of determination,  $R^2$ , related to the fitted model, indicating how close the

data provided fits the ideal model. This can indicate that a strong model fit is possible with temperature data from different integration times, as shown in Fig. 7, which also indicates a weaker fit generally for offset values of 0 and 1 (x-axis values 1–7, and 8–14 respectively). While integration time shows a strong variation in  $R^2$  between levels of 1000 and the other levels, their output diffusivity values shown in Fig. 6 – y-axis 50–54 respectively – shows a strong output correlation between integration times of 1000–2271. Integration time is an important factor since shorter values are required for faster frame rates, while longer integration times are required for lower temperatures. A low integration time at a given temperature may achieve a low saturation of the sensor. The range of saturation recommended by the manufacturer is 20–80%. From the manufacturer's software, an integration time of 1000  $\mu$ s, for a surface emissivity of 0.9 yields 5.3% saturation at 20 °C, and 7.5% at 30 °C. This is the range of sample surface temperatures during the post-flash heat diffusion event. Meanwhile at the same range, 4000  $\mu$ s provides 21.1% and 30.0% respectively. Objectively, the longest exposure from the set is the only one that meets the recommendations, however, as can be seen in Fig. 7, it produces the worst performance in matching ideal behaviour. However, for offsets of 2 and greater, with window limits 14 and greater, the integration times yield high  $R^2$  fits, with deviations at window limits of 30 and 40 (x-axis 20, 21, 27, 28, 34, and 35), with greater deviation introduced by integration time 1000  $\mu$ s. Consequently, two integration times of 2271 and 4000  $\mu$ s were selected for the main experiment, in order to reduce the total number of data captures, while capturing both demonstrable accuracy, and the objectively ideal setting in spite of its minor deviation.

The next parameter considered was flash power, ranging in four steps

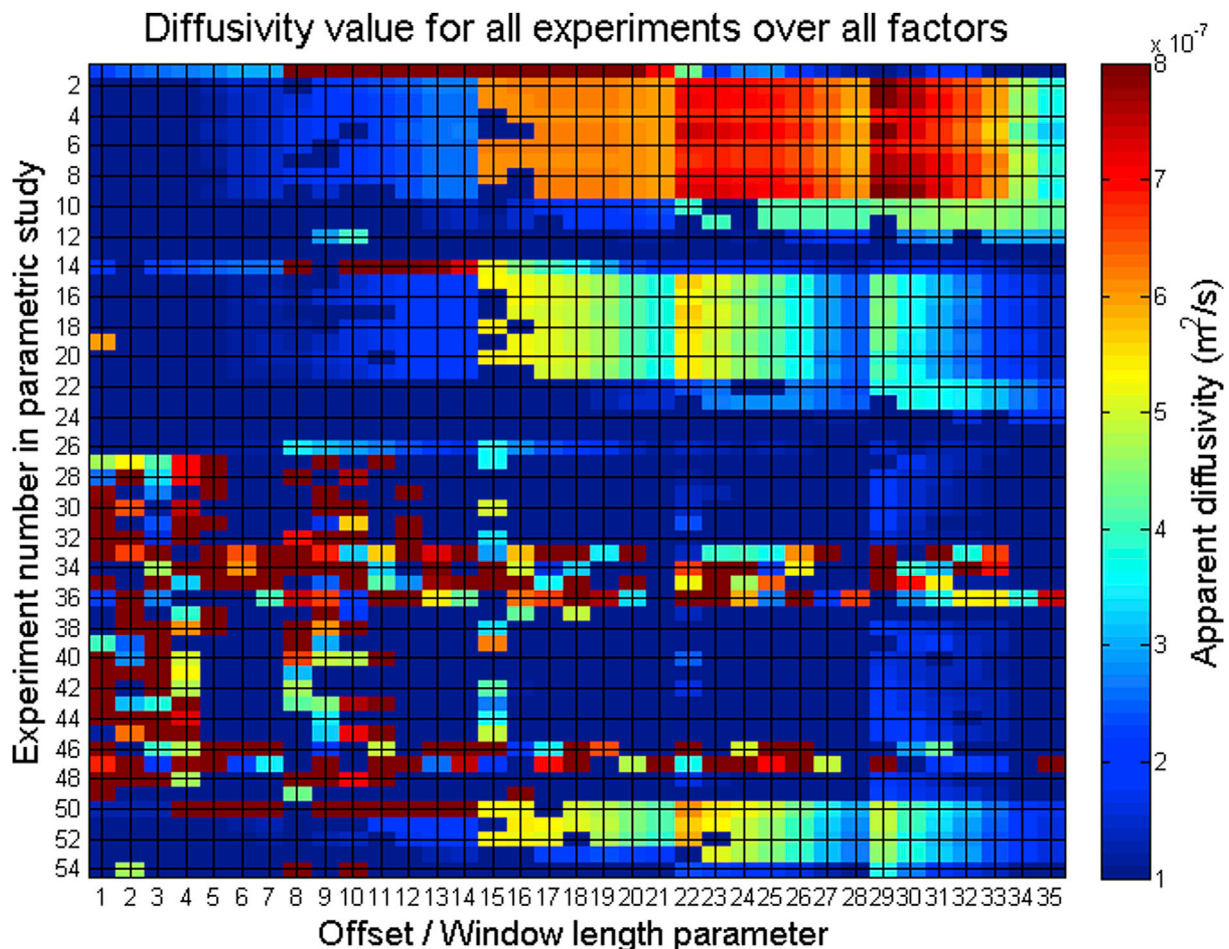


Fig. 6. Variation of estimated diffusivity values spread over experimental factors and levels such as integration time and flash power (y-axis) against variation in analysis factors and levels of frame offset and window size (x-axis).

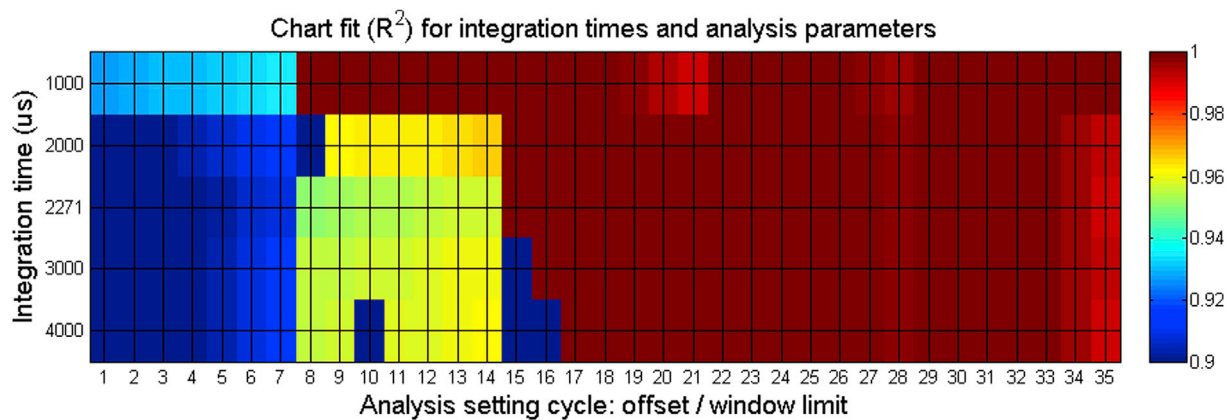


Fig. 7. Searching for stable settings using  $R^2$  indicating accuracy of fit of the two-layer model to the data under the given experimental conditions. Here is shown the  $R^2$  values for 5 experiments at 50% flash power over different integration times.

from 25 to 100%. In Fig. 8, it can be observed that lower flash powers attain a higher  $R^2$  parameter. However, it can also be observed with experiments 1, 14 and 26 of Fig. 6, where flash power of 25% is used, diffusivity is noisier and less stable, when compared to the following ten experiments in each case, where the other 3 flash power levels are used.

Finally, the application of soot coating is considered, and as seen in Fig. 9, the application of soot makes little difference to the  $R^2$  value for frame offsets 2–4, indicating a consistent fit of the model in either case. Additionally, there is some improvement of coefficient with increase in integration time, however this is exclusively in the 0–1 offset region that has already been excluded.

The experimental factors and their levels for analysis was narrowed down to a limited subset, which are shown in Table 2. All measurements were taken at 200 Hz.

#### 4.2. TBC ageing

The experiment was performed on a set of 6 EB-PVD YSZ TBC samples. All 6 samples were subjected to up to 128 h of oxidation ageing, with coatings failing between 80 and 128 h. For this experiment, only through-the-thickness diffusivity was measured due to the technical limitations of the experimental apparatus. The results are shown in Figs. 10 and 11.

As seen above, there is a sharp early drop in diffusivity in the soot-free inspections, which then levels, before increasing and decreasing once more at the end of coating life. However, the inspection with a soot coating applied shown below is completely free from this initial jump in values, while it still exhibits a later decrease after 16 h, and a similar short increase and decrease in diffusivity values at the end of the coating life.

#### 5. Discussion

Immediate observations from the results are that there is no unique relationship between diffusivity and coating age that would permit a one-point inspection randomly at any point in the sample's life to determine remaining useful life. However, it is noted that a trend is exhibited in diffusivity change that may be exploitable. In the case with soot coated samples the thermal diffusivity decreases, and then experiences an increase at around 96 h, before a final decrease. The late-life increase is also exhibited in non-soot coated samples. This pattern could be useful to diagnose the coating reaching the last stages of its life. With only a handful of samples surviving into the final decrease stage with the 16 h cycles used, the decrease itself could be more useful as an alarm indicating imminent failure, than as a feature of an ageing characterisation technique, unless more frequent inspections could be applied at the final stages to catch the onset of the terminal decline.

There are some notable differences between the inspections with and without soot coating. First of all, the tests without soot application exhibit a large initial jump that the coated inspections do not. This may be due to contamination of the coating from the initial application of soot exhibiting effects on the reflectance or apparent effusivity of the TBC that endures through an ultrasonic wash and the first 16 h furnace run. However, it could also be a result of the decrease in translucency TBCs undergo during service.

While there are consistent trends apparent over age, these exhibit a different shape, and are not as pronounced as trends identified by analysis of APS TBCs [8]. This may be related to the morphological structure differences between APS and EB-PVD, which could be investigated with a variation of experimental setup that can measure both the through-thickness and in-plane thermal diffusivities [16].

In both the soot coated and uncoated inspections, similar features of change are shown: an initial decrease, a gradual rise until 112 h, and a final drop before sample failure. Changes to thermal properties can be multi-faceted in their source. Thermal conductivity is influenced by point defects and grain boundaries of the ceramic [17]. Meanwhile, TBCs subject to sintering lose intra-columnar fine porosity, producing an increase in thermal conductivity during exposure at temperature. As the TGO layer grows under exposure, cavitation, rumpling and local interfacial separations form at the TGO and propagate over time, forming defects and obstructions to heat conduction [18]. Considering these factors, while non-soot coated TBCs undergo a rapid initial drop in apparent diffusivity, this is mirrored to a lesser extent in the soot coated inspections between 16 and 32 h, the cause of which will not simply be related to the semi-transparency of the TBC. With further sintering effects during ageing, an increase in diffusivity is expected, and is likely the source of the rise up to 96–112 h in both soot coated and uncoated inspections. Finally, a sudden drop in diffusivity prior to failure may coincide with the development of TGO growth, cavitation and interfacial cracks at the end of TBC life, which would shift the data away from the ideal two-layer model used.

One of the main flaws in this experiment is that the unpainted inspections are affected by the semi-transparency of TBCs, which are particularly prominent in the mid-wave IR band that has been used. This could be improved with use of a long-wave IR radiometer, or application of different fitting models that can accommodate for multiple layers [19], or semitransparency for emission as well as optical excitation [20,21]. In order to exploit these trends in service, these accommodations would need to be made, along with removing the effects of surface discolouration [14], while other techniques can be used to exploit the semi-transparent nature of TBCs, such as with mid-wave infrared reflectance imaging [22]. Data presented in this article may be accessed via Open Access [23].

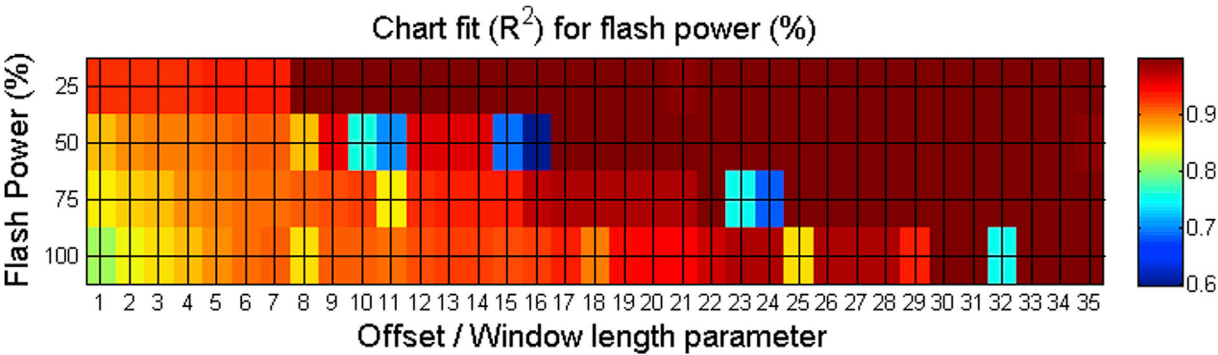


Fig. 8. Testing at constant integration time of 2271  $\mu$ s, are different levels of flash power tested for their  $R^2$  stability over different fitting parameters.

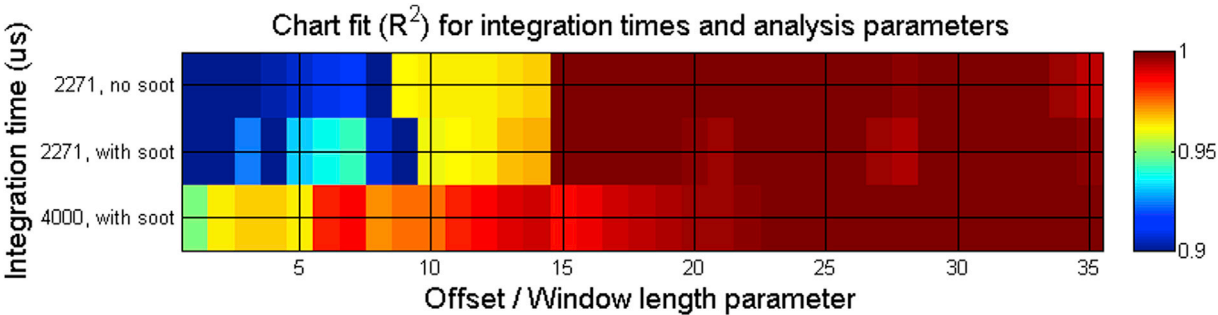


Fig. 9.  $R^2$  difference achieved without soot, compared to with soot, and with soot at the integration time of 4000  $\mu$ s. This shows that offset of 0 and 1 frame (x-axis 1–14) are particularly erroneous, resulting in poor fits of the model to the data.

Table 2  
Final experimental setup for furnace cycle experiment.

Factor	Name	Units	Levels	Levels
A	Integration time	$\mu$ s	1	2271
B	Flash intensity	% max power	1	50
C	Soot coating	Yes/No	2	Yes/No
D	Frame offset	number	1	2
E	Window limit	number	1	20

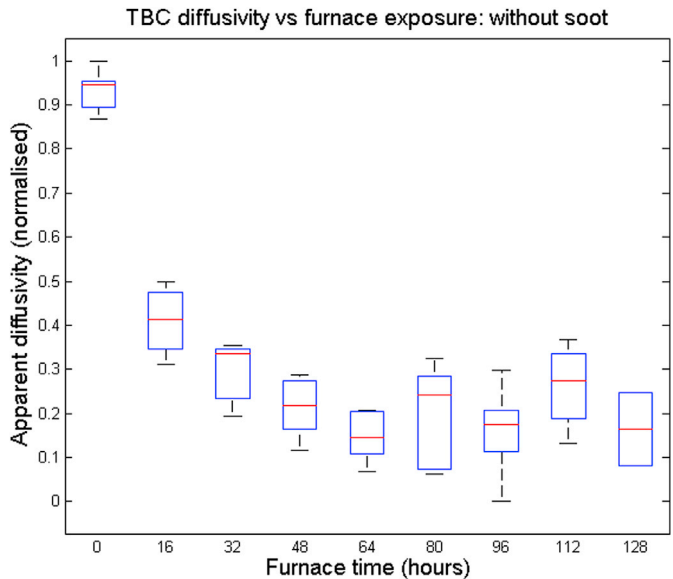


Fig. 10. Normalised diffusivity box plot of all samples over furnace exposure time, integration time 2271  $\mu$ s, flash power 50%, offset 2, frame limit 20, without soot, showing a pattern between the samples over ageing.

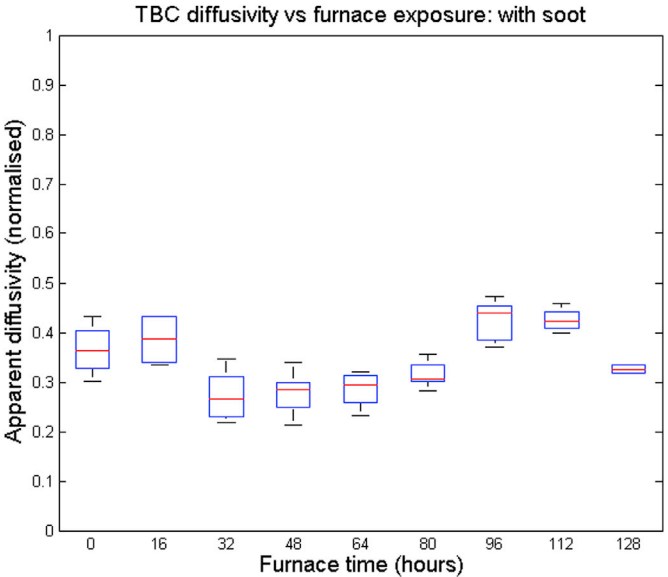


Fig. 11. Results for the same parameters, with soot coating, showing a similar late-age rise trend as without soot. The large step down from an initially high diffusivity has apparently disappeared, although a smaller initial decrease is present.

## 6. Conclusions

This paper has shown the application of the active thermographic flash method for determining through-thickness thermal diffusivity of six thin EB-PVD TBC samples in both the default condition and with an emissivity-improving soot coating applied. Under the limiting constraints of performing the flash test for through-thickness measurement of a fast thermal event, a parametric study for setting up the thermographic data

capture and analysis has been developed. The monitoring of thin EB-PVD TBCs during oxidation ageing has been undertaken, and has shown that the method is able to discern changes in through-thickness diffusivity over coating life, and that these changes are still observable without soot coating in the non-ideal performance of the test, even while the soot-free estimation will be inaccurate due to semi transparency. It is observed that there is not a unique relationship between through-thickness diffusivity value and ageing alone, where one range of measured values would translate directly into a range of life estimates, however, a history of measurements may be required for the part, in order to classify its age. The observed trends were not as clear as those observed by other researchers with APS TBCs, and this may be related to differences in through-thickness and laminar diffusivities, owing to EB-PVD TBCs' differing structure from APS TBCs. The thermal property changes observed provide three features of diffusivity trends that appear both in coated and uncoated inspections, and may be useful for estimation of coating life, while providing a marker that could indicate TBC close to the end of its life.

### Acknowledgements

This work has been financed by the UK Engineering and Physical Sciences Research Council through the EPSRC Centre in Through-life Engineering Services (grant no: EP/I033246/1) and the centre's industry partners.

### References

- [1] Boyce MP. An overview of gas turbines. In: Gas turbine engineering handbook. Third. Oxford, UK: Gulf Professional Publishing; 2006. p. 49.
- [2] Busso EP, Wright L, Evans HE, McCartney LN, Saunders SRJ, Osgerby S, et al. A physics-based life prediction methodology for thermal barrier coating systems. *Acta Mater* 2007;55:1491–503.
- [3] Beck T, Trunova O, Herzog R, Singheiser L. TBCs for gas turbines under thermomechanical loadings: failure behaviour and life prediction. In: EPJ web of conferences, vol. 33; 2012.
- [4] Pint BA, Wright IG, Lee WY, Zhang Y, Prüßner K, Alexander KB. Substrate and bond coat compositions: factors affecting alumina scale adhesion. *Mater Sci Eng A* 1998; 245(2):201–11.
- [5] Bison PG, Cernuschi F, Grinzato E, Marinetti S, Robba D. Ageing evaluation of thermal barrier coatings by thermal diffusivity. *Infrared Phys Technol* 2007;49(3): 286–91.
- [6] Bison P, Cernuschi F, Capelli S. A thermographic technique for the simultaneous estimation of in-plane and in-depth thermal diffusivities of TBCs. *Surf Coat Technol* 2011;205(10):3128–33.
- [7] Cernuschi F, Bison P, Marinetti S, Campagnoli E. Thermal diffusivity measurement by thermographic technique for the non-destructive integrity assessment of TBCs coupons. *Surf Coat Technol* 2010;205(2):498–505.
- [8] Cernuschi F, Capelli S, Bison P, Marinetti S, Lorenzoni L, Campagnoli E, et al. Non-destructive thermographic monitoring of crack evolution of thermal barrier coating coupons during cyclic oxidation ageing. *Acta Mater* 2011;59(16):6351–61.
- [9] Christensen RJ, Lipkin DM, Clarke DR. Nondestructive evaluation of the oxidation stresses through thermal barrier coatings using Cr piezospectroscopy. *NDT E Int* 1998;31(2):130.
- [10] Parker WJ, Jenkins RJ, Butler CP, Abbott GL. Flash method of determining thermal diffusivity, heat capacity, and thermal conductivity. *J Appl Phys* 1961;32:1679–84.
- [11] Thermal Wave Imaging Inc., Thermoscope II: advanced thermography for in-service inspection. [Online]. Available: [http://www.thermalwave.com/1/376/thermoscope\\_ii.asp](http://www.thermalwave.com/1/376/thermoscope_ii.asp). [Accessed 10 January 2016].
- [12] Bison PG, Cernuschi F, Grinzato E, Marinetti S, Robba D. Ageing evaluation of thermal barrier coatings by thermal diffusivity. *Infrared Phys Technol* 2007;49(3): 286–91.
- [13] Liebert CH. Emittance and absorptance of NASA ceramic thermal barrier coating system. In: NASA technical paper 1190; 1978.
- [14] Ptaszek G, Cawley P, Almond D, Pickering S. Transient thermography testing of unpainted thermal barrier coating (TBC) systems. *NDT E Int* 2013;59(C):48–56.
- [15] Shepard SM. "Reconstruction and enhancement of active thermographic image sequences. *Opt Eng* 2003;42(5):1337.
- [16] Bison P, Cernuschi F, Grinzato E. In-depth and in-plane thermal diffusivity measurements of thermal barrier coatings by IR camera: evaluation of ageing. *Int J Thermophys* 2008;29(6):2149–61.
- [17] Klemens PG, Gell M. Thermal conductivity of thermal barrier coatings. *Mater. Sci Eng A* 1998;245:143–9.
- [18] Clarke DR, Oechsner M, Padture NP. Thermal-barrier coatings for more efficient gas-turbine engines. *MRS Bull* 2012;37(10):891–8.
- [19] Akoshima M, Ogawa M, Baba T, Mizuno M. The thermal diffusivity measurement of the two layer ceramics using the laser flash method. *J High Temp Soc* 2008;34(5): 227–33.
- [20] Goldammer M, Baumann J. Analytical modeling of flash thermography results for a layered sample. *Nondestruct Eval Reliab Micro Nanomater Syst* 2002;4703:211–8.
- [21] Abuhamad M, Netzelmann U. Dual-band active thermography on infrared transparent materials. *Quant Infrared Thermogr J* 2010;7(2):189–200.
- [22] Eldridge JI, Spuckler CM, Martin RE. Monitoring delamination progression in thermal barrier coatings by mid-infrared reflectance imaging. *Int J Appl Ceram Technol* 2006;3(2):94–104.
- [23] Data underlying this study can be accessed through the Cranfield University repository at <http://dx.doi.org/10.17862/cranfield.rd.4985051>.



2017-08-03

# A study of pulsed thermography for life assessment of thin EB-PVD TBCs undergoing oxidation ageing

Tinsley, Lawrence

Elsevier

---

Tinsley L, Chalk C, Nicholls J, et al., (2017) A study of pulsed thermography for life assessment of thin EB-PVD TBCs undergoing oxidation ageing. NDT & E International, Volume 92, December 2017, pp. 67-74

<https://doi.org/10.1016/j.ndteint.2017.08.001>

*Downloaded from Cranfield Library Services E-Repository*